Multi-channel Enhanced Synchro-Reassignment Transform for Robust Identification of Sub/Super-Synchronous Oscillations Using Synchronized Measurements

Lixin Wang, Tianhong Niu, Zhenglong Sun, Han Gao, Shouqi Jiang, Guowei Cai, Tek Tjing Lie

***Abstract*—Synchrophasor-based sub-synchronous oscillations (SSOs) parameter identification is effective for monitoring SSOs, while its performance is significantly degraded by measurement noise, posing challenges to reliable parameter identification. This paper proposes a novel technique using multi-channel enhanced synchro-reassigning transform (MESRT) for robust and accurate SSO parameter identification. First, each measurement channel is transformed using the short-time Fourier transform (STFT) to construct a global multi-channel time-frequency (TF) representation. Then, an average modal energy-based strategy is developed to eliminate noise-induced spurious modes in the STFT spectrum. Subsequently, a three-step selection rule is applied to extract TF coefficients representing oscillation modes, from which the time-domain components are reconstructed. Finally, the Hilbert transform (HT) method is employed to identify the oscillation frequency and damping factor of each mode. The proposed MESRT method effectively improves the noise immunity and accuracy of conventional SRT by considering inter-channel correlations and leveraging modal energy to remove spurious modes. Case studies validate that the proposed method performs exceptionally well in terms of accuracy and noise robustness, demonstrating superior performance compared to existing methods.**

***Index Terms*—Sub/super-synchronous oscillations, parameter identification, multi-channel enhanced synchro-reassigning transform (MESRT), synchrophasor, noise.**

I. INTRODUCTION

In recent years, with the high penetration of renewable energy, sub-synchronous oscillations (SSOs) are being increasingly observed [1], [2]. Unlike traditional SSOs caused by the torsional dynamics of turbine generators, typically confined to a limited area, SSOs in renewable energy power systems involves the interactions between converter control systems and series-compensated transmission lines or weak AC grids, leading to widespread occurrences of SSOs globally [3]. Recently, the reported SSOs incidents were recorded in the Electric Reliability Council (ERCOT), southern Texas, USA [4], the Xcel Energy Network, Minnesota, USA [5], and the Guyam Power System, China [6]. As such oscillations have the potential to be highly destructive, they pose severe threats to equipment safety and power system stability. Therefore, rapid and accurate identification of oscillation parameters is of great importance to enable timely corrective actions.

With the widespread deployment of phasor measurement units (PMUs) and wide area measurement systems (WAMS) in modern power systems [7], the availability of high-resolution voltage and current data offers opportunities for SSO parameter identification. Existing measurement-based approaches can be broadly divided into frequency-domain, time-domain and time-frequency domain methods.

Frequency-domain methods are typically based on the discrete Fourier transform (DFT) and its improved variants, such as the improved interpolated DFT [8], window-optimized DFT [9], and iterative Taylor-based DFT [10]. These methods offer advantages of fast computation and ease of implementation. However, due to inherent limitations, their frequency resolution is constrained by the window length and is prone to spectral leakage and fence effects. Time-domain methods mainly include model-based parameter identification and mode decomposition techniques. The former identifies model parameters constructed from measurement data to identify oscillation parameters. Representative methods include the matrix pencil method (MPM) [11], the dynamic mode decomposition method (DMD) [12], and the Prony algorithm [13]. The latter decomposes oscillation signals into multiple modal components across different scales, from which the oscillation parameters are identified. Typical examples include variational mode decomposition (VMD) [14] and the fast independent component analysis (FastICA) [15]. However, these methods require a priori parameter settings, and their accuracy is highly sensitive to the selection of these parameters. Time-frequency domain methods identify parameters by exploiting both temporal and spectral characteristics of the signals. Representative methods include the short-time Fourier transform (STFT) [16] and continuous wavelet transform (CWT) [17]. However, constrained by the Heisenberg uncertainty principle, these approaches cannot simultaneously

This work was supported by the National Science Foundation of China under Grant 52507083. Lixin Wang, Tianhong Niu, Zhenglong Sun, Shouqi Jiang (corresponding author) and Guowei Cai are with the key Laboratory of Modern Power System Simulation and Control & Renewable Energy Technology, Ministry of Education, Northeast Electric Power University, Jilin, China (e-mail: wanglxnedu@163.com; 18843633338@163.com; nedusunzl@neepu.edu.cn; m15043264368@163.com; caigw@neepu.edu.cn); Han Gao is with the School of Electrical and Electronic Engineering, Harbin University of Science and Technology, Harbin 150080, China (Hannah 0323gh@hotmail.com); Tek Tjing Lie is with the Department of Electrical and Electronic Engineering, Auckland University of Technology (AUT), Auckland 1010, New Zealand (e-mail: tek.lie@aut.ac.nz).

achieve high resolution in both the time and frequency domains, limiting their identification accuracy. To address this issue, extensive research has been devoted to improving time-frequency concentration. In [18], the synchroextracting transform (SET) applies a synchro-extracting operator to enhance time-frequency energy concentration. In [19], the Fourier synchrosqueezed transform (FSST) further improves time-frequency resolution by compressing STFT coefficients toward their instantaneous frequencies. Based on [19], [20] further proposed the multisynchrosqueezing transform (MSST), which iteratively refines the time-frequency representation for superior concentration. Similarly, the synchrosqueezed wavelet transform (SWT) [21] further enhances the time-frequency resolution of the conventional CWT. However, these methods exhibit poor robustness under noisy conditions and often neglect couplings between sub- and super-synchronous components, resulting in inaccurate parameter identification.

Li *et al*. proposes the synchro-reassigning transform (SRT) [22], which inherits the advantages of time-frequency reassignment techniques, enhancing both the concentration and readability of time-frequency representations. The method shows excellent performance in analyzing strongly time-varying and nonstationary signals. Nevertheless, the extraction of local maxima in SRT is vulnerable to noise, leading to inaccurate peak identification. Moreover, as a single-channel approach, SRT fails to account for inter-channel correlations, which can affect mode identification accuracy. To improve robustness, the introduction of modal energy, which quantifies the energy contribution of each frequency band, provides an effective means to suppress noise and enhance the practical applicability of SRT.

This paper proposes a multi-channel enhanced SRT (MESRT)-based method for SSO parameter identification. First, each measurement channel undergoes STFT, and all measurements are mapped into a global multi-channel time-frequency matrix. Then, the average modal energy is calculated to eliminate noise-induced spurious modes. Subsequently, a three-step selection rule is applied to extract time-frequency coefficients representing oscillation modes. Finally, the time-domain components of each mode are constructed, and the oscillation frequency and damping factor are identified via the HT method. The main contributions of this paper are as follows:

(1) Unlike conventional model-based identification approaches, the proposed method is entirely data-driven and requires no prior knowledge of the oscillation or system model, which can adaptively decompose oscillation signals and accurately extract modal parameters.

(2) A novel multi-channel enhanced synchro-reassignment transform (MESRT) is proposed by extending the conventional single-channel SRT to a multi-channel cooperative framework. By exploiting cross-channel data redundancy and modal consistency, the proposed method suppresses measurement noise and enhances the robustness of time-frequency analysis. Compared with the single-channel SRT, it improves the reliability and consistency of oscillation mode extraction, yielding a more stable and concentrated time-frequency representation.

(3) A modal energy-based spurious mode elimination strategy is developed to mitigate the intrinsic sensitivity of SRT to noise-induced local extrema. By introducing average modal energy and relative modal energy weight to quantify the modal energy contribution of each frequency band, pseudo mode-related coefficients are removed from the time-frequency matrix before local maxima extraction. This ensures the consistency between the extracted modal trajectories and the true instantaneous frequency, thereby enhancing oscillation parameter estimation accuracy even under high-noise conditions.

(4) The effectiveness and robustness of the MESRT method are verified using synthetic signal, simulated data and actual measured data. MESRT exhibits superior performance in sub-/super-synchronous parameter extraction compared to the existing methods.

The remainder of this paper is organized as follows. Section II introduces the theoretical background of multi-channel measurements of sub/super-synchronous oscillation and reviews conventional SRT. Section III presents the proposed MESRT-based parameter identification scheme. Section IV verifies the effectiveness of the proposed method through case studies. Section V concludes this paper.

II. Theoretical Background

A. Multi-channel Measurements of Sub/super-synchronous Oscillation in Power Systems

The instantaneous voltage or current signal $x(t)$ in power systems during SSO can be expressed as [11]:

$$x(t) = A_0 \cos(2\pi f_0 t + \varphi_0) + \sum_{k=1}^{K} A_k \mathrm{e}^{\alpha_k t} \cos(2\pi f_k t + \varphi_k) + r(t) \quad (1)$$

where A_0, f_0, φ_0 are the amplitude, frequency and initial phase of the fundamental component respectively. K is the number of SSO modes. A_k, f_k, φ_k are the amplitude, frequency and initial phase of the k-th SSO component respectively; $r(t)$ represents the noise component.

In power systems, instantaneous voltage and current signals can be collected from high-speed synchronized data acquisition devices, such as point-on-wave measurement units. However, the observability of SSO modes varies significantly among different measurement channels. For instance, the same mode may exhibit a strong response in one measurement channel but a much weaker response in another, especially under high-noise conditions. Owing to these differences in modal observability among measurement channels, traditional single-channel identification methods may result in unreliable or inconsistent identification results. To address this issue, a multi-channel SSO analysis model is formulated to enable the simultaneous extraction of SSO modes from multiple channels. Taking current measurement signals as an example, the model can be expressed as:

$$\begin{cases} \boldsymbol{X}=\left[\boldsymbol{I}_i\right] \\ \boldsymbol{I}_i=\left\{I_i(t),\ t=1,2,\cdots,l;\ i=1,2,\cdots,m\right\} \\ I_i(t)=A_{I,i,0}\cos(2\pi f_{I,i,0}t+\varphi_{I,i,0}) \\ \quad +\sum_{k=1}^{K}A_{I,i,k}\mathrm{e}^{\alpha_{I,i,k}t}\cos(2\pi f_{I,i,k}t+\varphi_{I,i,k})+r_{I,i}(t) \end{cases} \tag{2}$$

where $\boldsymbol{I}_i$ denotes the current of branch i; l is the sample number; m represents the numbers of branches.

Therefore, the objective of SSO parameter identification is to extract oscillation modes from multi-channel measurements and determine the number of sub-synchronous modes K, along with their corresponding modal parameters, i.e., frequency (f), amplitude (A), damping factor (α) and phase (φ) for each mode.

B. Synchro-reassigning Transform (SRT)

Within a time window $u\in[t-\Delta u,\ t+\Delta u]$, the STFT of a single-mode signal $x(t)$ is given as [16]:

$$\boldsymbol{S}_x(t,\omega)=\int_{t-\Delta u}^{t+\Delta u}x(u)g(u-t)\mathrm{e}^{-\mathrm{j}\omega(u-t)}\mathrm{d}u \tag{3}$$

where Δu denotes half of the window size; $g(t)$ is the window function.

The STFT time-frequency matrix is expressed as:

$$\begin{aligned}\boldsymbol{S}_x(t,\omega)&=\left[\boldsymbol{S}_x(t,\omega_1)\quad \boldsymbol{S}_x(t,\omega_2)\quad \cdots\quad \boldsymbol{S}_x(t,\omega_n)\right]^{\mathrm{T}}\\&=\begin{bmatrix} S_x(t_1,\omega_1) & S_x(t_2,\omega_1) & \cdots & S_x(t_L,\omega_1)\\ S_x(t_1,\omega_2) & S_x(t_2,\omega_2) & \cdots & S_x(t_L,\omega_2)\\ \vdots & \vdots & & \vdots\\ S_x(t_1,\omega_k) & S_x(t_2,\omega_k) & \cdots & S_x(t_L,\omega_k)\\ \vdots & \vdots & & \vdots\\ S_x(t_1,\omega_n) & S_x(t_2,\omega_n) & \cdots & S_x(t_L,\omega_n)\end{bmatrix}\end{aligned} \tag{4}$$

According to the convolution theorem, (3) can be rewritten as:

$$\boldsymbol{S}_x(t,\omega)=\frac{1}{2\pi}\left(\hat{x}(\omega)*\left(\hat{g}(\omega)\mathrm{e}^{-\mathrm{j}\omega t}\right)\right)\mathrm{e}^{\mathrm{j}\omega t} \tag{5}$$

where $*$ denotes the convolution operation; $\hat{x}(\omega)$ and $\hat{g}(\omega)$ represent the Fourier transforms of $x(t)$ and $g(t)$ respectively.

Within the window $u\in[t-\Delta u,\ t+\Delta u]$, the single-mode signal $x(t)$ can be approximated as $x(t)\approx A_t\cos(\omega_t t+\varphi_0)$, and its Fourier transform is given by:

$$\hat{x}(\omega)=\pi A_t\delta(\omega-\omega_t)\mathrm{e}^{\mathrm{j}\varphi_0} \tag{6}$$

where A_t and ω_t denote the instantaneous amplitude and frequency at time t; $\delta(\cdot)$ represents the Dirac function; φ_0 is the constant phase.

Substituting (6) into (5) yields:

$$\begin{aligned}\left|\boldsymbol{S}_x(t,\omega)\right|&=\left|A_t\delta(\omega-\omega_t)*\hat{g}(\omega)\right|/2\\&=\left|A_t\hat{g}(\omega-\omega_t)\right|/2\end{aligned} \tag{7}$$

For a general multimode signal, considering the linearity of the STFT, (7) can be extended as:

$$\left|\boldsymbol{S}_x(t,\omega)\right|=\sum_{i=1}^{n}\left|A_{t,i}\hat{g}(\omega-\omega_{t,i})\right|/2 \tag{8}$$

where $A_{t,i}$ and $\omega_{t,i}$ represent the amplitude and instantaneous frequency of the i-th mode at time t respectively.

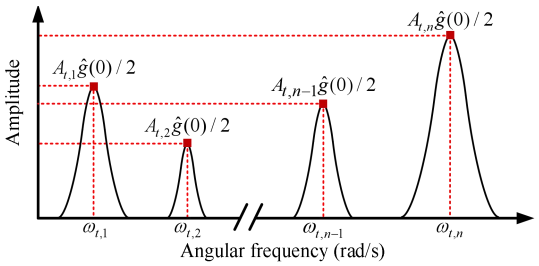

Fig. 1. Illustration of the STFT spectrum at time t.

By comparing (7) and (8), $|\boldsymbol{S}_x(t,\omega)|$ in (8) can be obtained by shifting and scaling $\hat{g}(\omega)$ along frequency trajectories $\omega_{t,i}$ with corresponding amplitudes $A_{t,i}/2$, as shown in Fig. 1.

According to the above analysis, the signal energy in the time-frequency domain is concentrated around the modal frequencies $\omega_{t,i}$, while a certain degree of energy dispersion occurs due to the frequency-smearing effect inherent in STFT. To mitigate this effect, the local maxima of $|\boldsymbol{S}_x(t,\omega)|$ at each instant are extracted to identify the instantaneous frequency trajectories. This process forms the foundation of the SRT, enabling high-precision time-frequency representation of SSO signals. To achieve this, a three-step selection rule is applied to determine the local maxima of $|\boldsymbol{S}_x(t,\omega)|$.

First, the first-order partial derivative of $|\boldsymbol{S}_x(t,\omega)|$ in (3) with respect to ω is calculated as:

$$\frac{\partial\left|\boldsymbol{S}_x(t,\omega)\right|}{\partial\omega}=\frac{\left(\mathrm{Re}(\boldsymbol{S}_x)\cdot\dfrac{\partial\mathrm{Re}(\boldsymbol{S}_x)}{\partial\omega}+\mathrm{Im}(\boldsymbol{S}_x)\cdot\dfrac{\partial\mathrm{Im}(\boldsymbol{S}_x)}{\partial\omega}\right)}{\left|\boldsymbol{S}_x(t,\omega)\right|} \tag{9}$$

where $\mathrm{Re}(\boldsymbol{S}_x)$ and $\mathrm{Im}(\boldsymbol{S}_x)$ denote the real and imaginary parts of $|\boldsymbol{S}_x(t,\omega)|$ respectively.

The derivatives of $\partial\mathrm{Re}(\boldsymbol{S}_x)/\partial\omega$ and $\partial\,\mathrm{Im}(\boldsymbol{S}_x)/\partial\omega$ in (9) are obtained by differentiating (3) with respect to ω:

$$\begin{aligned}\boldsymbol{S}'_{x,\omega}(\omega,t)&=\frac{\partial\boldsymbol{S}_x(t,\omega)}{\partial\omega}=\frac{\partial\,\mathrm{Re}(\boldsymbol{S}_x)}{\partial\omega}+\mathrm{j}\,\frac{\partial\,\mathrm{Im}(\boldsymbol{S}_x)}{\partial\omega}\\&=\int_{-\infty}^{+\infty}-\mathrm{j}(u-t)\cdot x(u)\,g(u-t)\,e^{-\mathrm{j}\omega(u-t)}\mathrm{d}u\\&=\mathrm{Re}(\boldsymbol{S}'_{x,\omega})+\mathrm{j}\,\mathrm{Im}(\boldsymbol{S}'_{x,\omega})\end{aligned} \tag{10}$$

where $\mathrm{Re}(\boldsymbol{S}'_{x,\omega})$ and $\mathrm{Im}(\boldsymbol{S}'_{x,\omega})$ denote the real and imaginary parts of $\boldsymbol{S}'_{x,\omega}$.

Substituting (10) into (9) gives:

$$\frac{\partial\left|\boldsymbol{S}_x(t,\omega)\right|}{\partial\omega}=\frac{\left(\mathrm{Re}(\boldsymbol{S}_x)\cdot\mathrm{Re}(\boldsymbol{S}'_{x,\omega})+\mathrm{Im}(\boldsymbol{S}_x)\cdot\mathrm{Im}(\boldsymbol{S}'_{x,\omega})\right)}{\left|\boldsymbol{S}_x(t,\omega)\right|} \tag{11}$$

To obtain the local maxima of $|\boldsymbol{S}_x(t,\omega)|$ along the frequency direction at a given time t, the discrete forms of (3), (10) and (11) are written as:

$$\boldsymbol{S}_x(\tau,\eta)=\sum_{l=0}^{L-1}s(l)g(l-\tau)e^{-\mathrm{j}\eta\frac{l-\tau}{L}} \tag{12}$$

$$\boldsymbol{S}'_{x,\omega}(\tau,\eta)=\sum_{l=0}^{L-1}-\mathrm{j}(l-\tau)\cdot s(l)g(l-\tau)e^{-\mathrm{j}\eta\frac{l-\tau}{L}} \tag{13}$$

$$\frac{\partial\left|\boldsymbol{S}_x(\tau,\eta)\right|}{\partial\eta}=\frac{\begin{pmatrix}\mathrm{Re}(\boldsymbol{S}_x(\tau,\eta))\cdot\mathrm{Re}(\boldsymbol{S}'_{x,\omega}(\tau,\eta))\\+\mathrm{Im}(\boldsymbol{S}_x(\tau,\eta))\cdot\mathrm{Im}(\boldsymbol{S}'_{x,\omega}(\tau,\eta))\end{pmatrix}}{\left|\boldsymbol{S}_x(\tau,\eta)\right|} \tag{14}$$

where η denotes the discrete frequency center; L is the window size; τ denotes the discrete time index.

Based on (12)-(14), the three-step selection rule is further defined as follows [22].

First, $|\boldsymbol{S}_x(t,\omega)|$ reaches a local maximum at the discrete time-frequency point (τ, η), satisfying:

$$\begin{cases}\left|\boldsymbol{S}_x(\tau,\eta-1)\right|\le\left|\boldsymbol{S}_x(\tau,\eta)\right|\\ \left|\boldsymbol{S}_x(\tau,\eta+1)\right|\le\left|\boldsymbol{S}_x(\tau,\eta)\right|\end{cases} \tag{15}$$

Second, the first-order derivative of $|\boldsymbol{S}_x(t,\omega)|$ with respect to the discrete frequency η equals zero:

$$\begin{cases}\left|\dfrac{\partial\left|\boldsymbol{S}_x(\tau,\eta)\right|}{\partial\eta}\right|<e_{\mathrm{cal}}\\ \left|\dfrac{\partial\left|\boldsymbol{S}_x(\tau,\eta)\right|}{\partial\eta}\right|\le\left|\dfrac{\partial\left|\boldsymbol{S}_x(\tau,\eta-1)\right|}{\partial(\eta-1)}\right|\\ \left|\dfrac{\partial\left|\boldsymbol{S}_x(\tau,\eta)\right|}{\partial\eta}\right|\le\left|\dfrac{\partial\left|\boldsymbol{S}_x(\tau,\eta+1)\right|}{\partial(\eta+1)}\right|\end{cases} \tag{16}$$

where e_{cal} denotes the calculation error, set to 10 in this research.

Third, the second-order derivative is negative, satisfying:

$$\begin{cases}\dfrac{\partial\left|\boldsymbol{S}_x(\tau,\eta)\right|}{\partial\eta}<\dfrac{\partial\left|\boldsymbol{S}_x(\tau,\eta-1)\right|}{\partial(\eta-1)}\\ \dfrac{\partial\left|\boldsymbol{S}_x(\tau,\eta)\right|}{\partial\eta}>\dfrac{\partial\left|\boldsymbol{S}_x(\tau,\eta+1)\right|}{\partial(\eta+1)}\end{cases} \tag{17}$$

By applying (15)-(17), all local maxima across time centers can be accurately obtained. Only the coefficients in (4) that are associated with the instantaneous frequency trajectories are preserved, while the rest are set to 0, resulting in a sparse time-frequency matrix $\boldsymbol{SRT}_x(t,\omega)$ that contains only sub/super-synchronous oscillation modes, as expressed in (18) and (19).

$$\boldsymbol{SRT}_x(t,\omega)=\begin{cases}\boldsymbol{S}_x(t,\omega), & \text{satisfying (15)}-\text{(17)}\\ 0, & \text{not satisfying (15)}-\text{(17)}\end{cases} \tag{18}$$

$$\boldsymbol{SRT}_x(t,\omega)=\begin{bmatrix}0&0&\cdots&0\\ \vdots&\vdots&&\vdots\\ S_x(t_1,\omega_{p-1})&S_x(t_2,\omega_{p-1})&\cdots&S_x(t_L,\omega_{p-1})\\ S_x(t_1,\omega_p)&S_x(t_2,\omega_p)&\cdots&S_x(t_L,\omega_p)\\ \vdots&\vdots&&\vdots\\ S_x(t_1,\omega_{q-1})&S_x(t_2,\omega_{q-1})&\cdots&S_x(t_L,\omega_{q-1})\\ S_x(t_1,\omega_q)&S_x(t_2,\omega_q)&\cdots&S_x(t_L,\omega_q)\\ \vdots&\vdots&&\vdots\\ 0&0&\cdots&0\end{bmatrix} \tag{19}$$

where $S_x(t_L, \omega_p)$ represents the retained STFT coefficient of $\boldsymbol{S}_x(t,\omega)$ corresponding to the sub/super-synchronous oscillation modes at time t_L and frequency ω_p.

III. Multi-channel Enhanced SRT and Sub/super-Synchronous Oscillation Identification

In practice, measurement signals are often contaminated by noise, which can introduce spurious modes and generate local extrema that mislead the three-step selection procedure of SRT, thereby causing deviations in the extracted modal trajectories. Moreover, conventional SRT is inherently a single-channel method and cannot simultaneously extract sub/super-synchronous components from multi-channel measurements. To address these limitations, a noise-robust mode removal scheme is developed for SRT, and as an extension, the MESRT is proposed to process multi-channel measurements simultaneously, enabling accurate identification of sub/super-synchronous oscillation modes.

A. Multi-channel Enhanced SRT (*MESRT*)

Let the measurement matrix $\boldsymbol{I}$, comprising current data from N channels, be expressed as:

$$\boldsymbol{I}=\begin{bmatrix}\boldsymbol{I}_1\\ \boldsymbol{I}_2\\ \vdots\\ \boldsymbol{I}_N\end{bmatrix}^{\mathrm{T}}=\begin{bmatrix}I_{1,1}&I_{1,2}&\cdots&I_{1,L}\\ I_{2,1}&I_{2,2}&\cdots&I_{2,L}\\ \vdots&\vdots&\ddots&\vdots\\ I_{N,1}&I_{N,2}&\cdots&I_{N,L}\end{bmatrix}^{\mathrm{T}} \tag{20}$$

The STFT is applied to each channel individually, producing time-frequency representation in the form:

$$\begin{aligned}\boldsymbol{S}_r(t,\omega)&=\begin{bmatrix}\boldsymbol{S}_r(t,\omega_1)&\boldsymbol{S}_r(t,\omega_2)&\cdots&\boldsymbol{S}_r(t,\omega_n)\end{bmatrix}^{\mathrm{T}}\\ &=\begin{bmatrix}S_r(t_1,\omega_1)&S_r(t_2,\omega_1)&\cdots&S_r(t_L,\omega_1)\\ S_r(t_1,\omega_2)&S_r(t_2,\omega_2)&\cdots&S_r(t_L,\omega_2)\\ \vdots&\vdots&&\vdots\\ S_r(t_1,\omega_k)&S_r(t_2,\omega_k)&\cdots&S_r(t_L,\omega_k)\\ \vdots&\vdots&&\vdots\\ S_r(t_1,\omega_n)&S_r(t_2,\omega_n)&\cdots&S_r(t_L,\omega_n)\end{bmatrix}\end{aligned} \tag{21}$$

where $S_r(t_L, \omega_n)$ (r=1, 2 ,....., N) denotes the STFT coefficient of channel $\boldsymbol{I}_r$ at time instant t_L and discrete frequency ω_n.

Based on (21), a global multi-channel time-frequency matrix is constructed to capture inter-channel correlations and facilitate the extraction sub/super-synchronous modes, as [23]:

$$\begin{aligned}&\begin{cases}\boldsymbol{S}^{multi}(t,\omega)=\left\{\left\{\left|\boldsymbol{S}_1(t,\omega)\right|^2+\left|\boldsymbol{S}_2(t,\omega)\right|^2+\cdots+\left|\boldsymbol{S}_N(t,\omega)\right|^2\right\}\right\}^{1/2}\\ \boldsymbol{S}^{multi}(t,\omega)=\begin{bmatrix}\boldsymbol{S}^{multi}(t,\omega_1)&\boldsymbol{S}^{multi}(t,\omega_2)&\cdots&\boldsymbol{S}^{multi}(t,\omega_n)\end{bmatrix}^{\mathrm{T}}\end{cases}\\ &=\begin{bmatrix}S^{multi}(t_1,\omega_1)&S^{multi}(t_2,\omega_1)&\cdots&S^{multi}(t_L,\omega_1)\\ S^{multi}(t_1,\omega_2)&S^{multi}(t_2,\omega_2)&\cdots&S^{multi}(t_L,\omega_2)\\ \vdots&\vdots&&\vdots\\ S^{multi}(t_1,\omega_k)&S^{multi}(t_2,\omega_k)&\cdots&S^{multi}(t_L,\omega_k)\\ \vdots&\vdots&&\vdots\\ S^{multi}(t_1,\omega_n)&S^{multi}(t_2,\omega_n)&\cdots&S^{multi}(t_L,\omega_n)\end{bmatrix}\end{aligned} \tag{22}$$

where $S^{multi}(t_L, \omega_n)$ denotes the global STFT coefficient of measurement matrix $\boldsymbol{I}$ at time instant t_L and frequency ω_n.

To eliminate noise-induced spurious modes in (22), the mean

modal energy (MME) is adopted, as MME is generally higher for sub/super-synchronous modes than for noise components. The MME associated with frequency ω_k is defined as:

$$\gamma_k = \frac{1}{L}\sum_{t=1}^{L} \boldsymbol{S}^{multi}(t,\omega_k)^2 \tag{23}$$

where $\boldsymbol{S}^{multi}(t, \omega_k)$ denotes the STFT coefficient of $\boldsymbol{S}^{multi}(t, \omega)$ at frequency ω_k.

And the relative modal energy weight is calculated by:

$$\mu(k) = \gamma_k / (\sum_{k=1}^{n} \gamma_k) \tag{24}$$

where μ_k is the relative modal energy weight; n is the number of rows in $\boldsymbol{S}^{multi}(t, \omega)$.

If $\mu(k)$ is smaller than a predefined threshold μ_0, the corresponding frequency ω_k is considered as a noise-induced spurious mode, and $\boldsymbol{S}^{multi}(t, \omega_k)$ in (22) is set to 0. The selection of μ_0 is critical: a larger μ_0 may lead to the omission of dominant sub/super-synchronous modes, whereas a smaller value may retain irrelevant noise components. Typically, μ_0=0.02 is adopted to ensure accurate mode identification.

After eliminating noise components, the refined time-frequency representation in (22) is expressed as $\tilde{\boldsymbol{S}}^{multi}(t,\omega)$:

$$\tilde{\boldsymbol{S}}^{multi}(t,\omega)=\begin{bmatrix} \tilde{S}^{multi}(t_1,\omega_1) & \tilde{S}^{multi}(t_2,\omega_1) & \cdots & \tilde{S}^{multi}(t_L,\omega_1) \\ \vdots & \vdots & \vdots & \vdots \\ 0 & 0 & 0 & 0 \\ \vdots & \vdots & \vdots & \vdots \\ \tilde{S}^{multi}(t_1,\omega_{p-1}) & \tilde{S}^{multi}(t_2,\omega_{p-1}) & \cdots & \tilde{S}^{multi}(t_L,\omega_{p-1}) \\ \tilde{S}^{multi}(t_1,\omega_p) & \tilde{S}^{multi}(t_2,\omega_p) & \cdots & \tilde{S}^{multi}(t_L,\omega_p) \\ \vdots & \vdots & & \vdots \\ \tilde{S}^{multi}(t_1,\omega_{q-1}) & \tilde{S}^{multi}(t_2,\omega_{q-1}) & \cdots & \tilde{S}^{multi}(t_L,\omega_{q-1}) \\ \tilde{S}^{multi}(t_1,\omega_q) & \tilde{S}^{multi}(t_2,\omega_q) & \cdots & \tilde{S}^{multi}(t_L,\omega_q) \\ \vdots & \vdots & & \vdots \\ 0 & 0 & 0 & 0 \\ \vdots & \vdots & \vdots & \vdots \\ \tilde{S}^{multi}(t_1,\omega_n) & \tilde{S}^{multi}(t_2,\omega_n) & \cdots & \tilde{S}^{multi}(t_L,\omega_n) \end{bmatrix} \tag{25}$$

Similar to (3), the TF representation $\tilde{\boldsymbol{S}}^{multi}(t,\omega)$ after removing spurious modes can be expressed as:

$$\tilde{\boldsymbol{S}}^{multi}(t,\omega) = \int_{-\infty}^{+\infty} \tilde{x}(u) g(u-t) \mathrm{e}^{-\mathrm{j}\omega(u-t)} \mathrm{d}u \tag{26}$$

where $\tilde{x}(t)$ denotes the time-domain signal reconstructed by the inverse STFT of $\tilde{\boldsymbol{S}}^{multi}(t,\omega)$.

Following the SRT procedure described in Section II.B, a new sparse TF matrix similar to (19) is obtained:

$$\widetilde{\boldsymbol{SRT}}^{multi}(t,\omega)=\begin{bmatrix} 0 & 0 & \cdots & 0 \\ \vdots & \vdots & & \vdots \\ \tilde{S}^{multi}(t_1,\omega_p) & \tilde{S}^{multi}(t_2,\omega_p) & \cdots & \tilde{S}^{multi}(t_L,\omega_p) \\ \vdots & \vdots & & \vdots \\ \tilde{S}^{multi}(t_1,\omega_q) & \tilde{S}^{multi}(t_2,\omega_q) & \cdots & \tilde{S}^{multi}(t_L,\omega_q) \\ \vdots & \vdots & & \vdots \\ 0 & 0 & \cdots & 0 \end{bmatrix} \tag{27}$$

Comparison of (19) and (27) highlights that the MESRT, by eliminating spurious modes, applying the three-step selection rule, and considering inter-channel correlations, retains only the coefficients corresponding to real sub/super-synchronous modes, significantly enhancing the time-frequency resolution.

B. Mode Component Reconstruction

A multi-mode coupled oscillation signal $x_m(t)$ can generally be expressed as:

$$x_m(t) \approx \sum_{i=1}^{n} A_i(t) \mathrm{e}^{\mathrm{j}(\varphi'_i(t)t+\varphi_{0,i}(t))} \tag{28}$$

where $A_i(t)$, $\varphi'_i(t)$ and $\varphi_{0,i}(t)$ denote the instantaneous amplitude, frequency, and locally constant phase term associated with the time center t of the i-th mode, respectively; n is the number of modes.

The STFT of $x_m(t)$ is given by [24]:

$$\boldsymbol{S}_{x_m}(t,\omega) = \frac{1}{2}\sum_{i=1}^{n} A_i(t)\hat{g}(\omega-\varphi'_i(t)) \mathrm{e}^{\mathrm{j}(\varphi'_i(t)t+\varphi_{0,i}(t))} \tag{29}$$

According to Section II.B and III.A, instantaneous amplitudes and frequencies can be extracted from $\tilde{\boldsymbol{S}}^{multi}(t,\omega)$ by locating local maximum. Therefore, the sparse time-frequency matrix $\widetilde{\boldsymbol{SRT}}_{x_m}^{multi}(t,\varphi_i'(t))$ can be written as:

$$\begin{aligned} \sum_{i=1}^{n} \widetilde{\boldsymbol{SRT}}_{x_m}^{multi}(t,\varphi_i'(t)) &= \boldsymbol{S}_{x_m}(t,\omega)\Big|_{\omega=\varphi'_i(t)} \\ &= \frac{1}{2}\sum_{i=1}^{n} A_i(t)\hat{g}(0)\mathrm{e}^{\mathrm{j}(\varphi'_i(t)t+\varphi_{0,i}(t))} \end{aligned} \tag{30}$$

Comparing (28) and (30), we can obtain:

$$x_m(t) = \sum_{i=1}^{n} x_i(t) = \sum_{i=1}^{n} \widetilde{\boldsymbol{SRT}}_{x_m}^{multi}(t,\varphi'_i(t)) / (\hat{g}(0)/2) \tag{31}$$

With the $\widetilde{\boldsymbol{SRT}}_{x_m}^{multi}(t,\varphi'_i(t))$ of i-th mode expressed as:

$$\widetilde{\boldsymbol{SRT}}_{x_m}^{multi}(t,\varphi'_i(t)) = \begin{bmatrix} 0 & 0 & \cdots & 0 \\ \vdots & \vdots & & \vdots \\ 0 & 0 & \cdots & 0 \\ \tilde{S}_{x_m}^{multi}(t_1,\omega_i) & \tilde{S}_{x_m}^{multi}(t_2,\omega_i) & \cdots & \tilde{S}_{x_m}^{multi}(t_L,\omega_i) \\ 0 & 0 & \cdots & 0 \\ \vdots & \vdots & & \vdots \\ 0 & 0 & \cdots & 0 \end{bmatrix} \tag{32}$$

The $\widetilde{\boldsymbol{SRT}}_{x_m}^{multi}(t,\varphi'_i(t))$ in (32) represents the subset of time-

frequency coefficients in (27) associated with mode ω_i, while the remaining coefficients are set to 0.

C. Parameter Identification Using the Hilbert Transform

The Hilbert transform is applied to the mono-frequency mode $x_i(t)$ obtained by MESRT, which is given by [25]:

$$x_i^*(t)=\frac{1}{\pi}P\int_{-\infty}^{+\infty}\frac{x_i(\tau)}{t-\tau}\mathrm{d}\tau \tag{33}$$

where P denotes the Cauchy principal value.

The analytic signal of $x_i(t)$ is then constructed as:

$$z_i(t)=x_i(t)+\mathrm{j}x_i^*(t)=A_i(t)\mathrm{e}^{\mathrm{j}\varphi_i(t)} \tag{34}$$

where $A_i(t)$ and $\varphi_i(t)$ are the instantaneous amplitude and instantaneous phase respectively; The instantaneous frequency $f_i(t)$ is obtained by differentiating $\varphi_i(t)$:

$$\begin{cases} A_i(t)=\sqrt{x_i^2(t)+x_i^{*2}(t)} \\ \varphi_i(t)=\arctan\dfrac{x_i^*(t)}{x_i(t)} \\ f_i(t)=\dfrac{1}{2\pi}\dfrac{\mathrm{d}\varphi_i(t)}{\mathrm{d}t} \end{cases} \tag{35}$$

If the system has an eigenvalue $\sigma_i=-\lambda_i\pm\mathrm{j}\omega_i$, its oscillatory response in the time domain can be expressed as:

$$F_i(t)=A_{i0}e^{-\lambda_i t}\cos(2\pi f_i t+\varphi_{i0}) \tag{36}$$

where A_{i0}, λ_i, ω_i and φ_{i0} are initial amplitude, damping factor, oscillation angular frequency and phase angle respectively.

Combining (34) and (36) yields:

$$\begin{cases} \ln A_i(t)=-\lambda_i t+\ln A_{i0} \\ \varphi_i(t)=2\pi f_i t+\varphi_{i0} \end{cases} \tag{37}$$

By applying least-squares fitting to (37), the sub/super-synchronous oscillation parameters (namely, oscillation frequency f_i and damping factor λ_i) can be identified from the multi-channel measurement data.

D. Framework of the Proposed Method

Algorithm 1 Implementation procedure of the MESRT method

1). Input current data $\boldsymbol{I}=[\boldsymbol{I}_1, \boldsymbol{I}_2, \cdots, \boldsymbol{I}_N]$ collected from PMUs.
2). Apply STFT to each current and obtain STFT coefficient matrix $\boldsymbol{S}_r(t,\omega)$ $(i=1,2,\cdots,N)$ of each current by (21).
3). Calculate global time-frequency matrix $\boldsymbol{S}^{multi}(t,\omega)$ by (22).
4). Calculate the relative modal energy weight of each mode by (23) and (24).
5). Eliminate noise-induced spurious modes and achieve the TF matrix without spurious modes as (25).
6). Apply the three-step selection rule (15)-(17), and obtain the sparse TF matrix in (27) containing only the sub/super-synchronous oscillation modes.
7). Reconstruct the time-domain components of each sub/super-synchronous oscillation mode using (31).
8). Identify mode parameters, e.g., oscillation frequency f_i, and damping factor λ_i associated with the extracted sub/super-synchronous modes by (37).

Based on the above analysis, the proposed MESRT method identifies the oscillation frequency and damping factor of sub-/super-synchronous oscillation modes from multi-channel measurements. By incorporating inter-channel correlations, MESRT ensures synchronous and accurate extraction of modal parameters. Moreover, the combination of average modal energy and the three-step selection rule significantly improve the time-frequency energy concentration. The main steps of the proposed method are summarized in **Algorithm 1**.

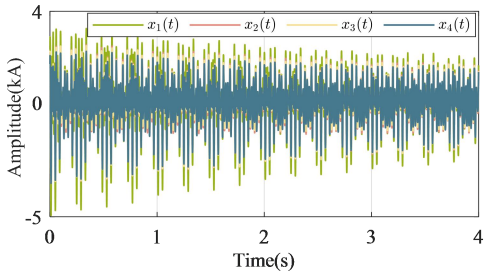

Fig. 2. Waveform of the synthetic signal.

TABLE I
PARAMETERS OF THE SYNTHETIC SIGNAL

	Mode	α	f/Hz	φ/rad
sub-synchronous	1	0.3	25	π/2
	2	0.2	29	π/3
super-synchronous	3	0.2	71	-π/4
	4	0.3	75	-π/2

IV. CASE STUDIES

In this section, the performance of the proposed MESRT method is evaluated using synthetic signal, simulated signal and actual measured data from the North China power grid [8]. Comparative analysis with STFT, SET, FSST, conventional SRT and multi-channel Prony (MProny) methods are also conducted to validate the superiority of the proposed method. The identification results are evaluated using the relative error (RE), defined according to IEEE standard [26] as:

$$\mathrm{RE}=\frac{|\hat{p}-p|}{p}\times 100\% \tag{38}$$

where $\hat{p}$ and p denote the theoretical and identified parameters.

A. Synthetic Signals

The synthetic signal, comprising two sub-synchronous components, two super-synchronous components, and a fundamental frequency component, is represented as:

$$\begin{cases} s_1(t)=e^{-\alpha_{\mathrm{sub},1}t}\cos(2\pi f_{\mathrm{sub},1}t+\varphi_{\mathrm{sub},1}) \\ s_2(t)=e^{-\alpha_{\mathrm{sub},2}t}\cos(2\pi f_{\mathrm{sub},2}t+\varphi_{\mathrm{sub},2}) \\ s_3(t)=e^{-\alpha_{\mathrm{sup},3}t}\cos(2\pi f_{\mathrm{sup},3}t+\varphi_{\mathrm{sup},3}) \\ s_4(t)=e^{-\alpha_{\mathrm{sup},4}t}\cos(2\pi f_{\mathrm{sup},4}t+\varphi_{\mathrm{sup},4}) \end{cases} \tag{39}$$

where (α_{sub}, φ_{sub}, f_{sub}) and (α_{sup}, φ_{sup}, f_{sup}) are, respectively, damping factors, phases and frequencies of the sub-synchronous and super-synchronous components, with their parameters listed in Table I. It should be noted that, the amplitudes of each modal component defined in (39) are constructed with unit amplitude, since the purpose of this case is to verify the identification accuracy of oscillation frequency and damping factor. The amplitude variations observed in the

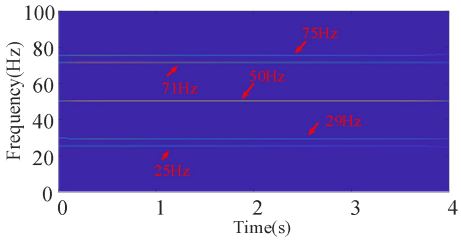

Fig. 3. Time-frequency analysis results of $\boldsymbol{X}$ using MESRT.

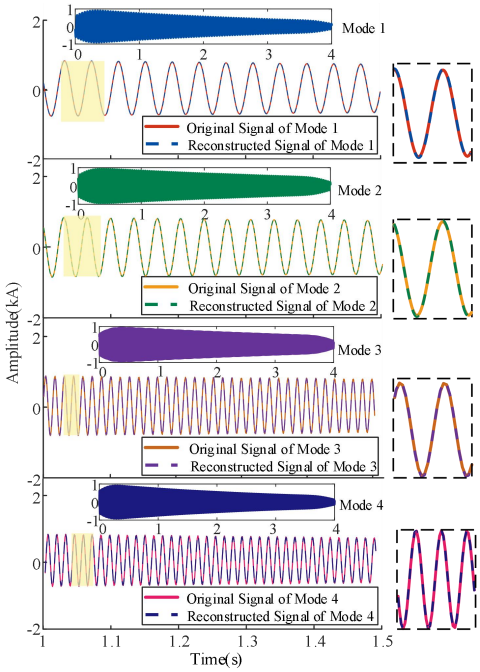

Fig. 4. Comparison of reconstructed and original signals for each mode.

multi-channel signals are introduced through the linear mixing process described in (40).

The constructed multi-channel signal matrix $\boldsymbol{X}$ in (40) is formulated by coupling sub/super-synchronous components defined in (39). To simulate a harsher noise environment, the signal-to-noise ratio (SNR) of the synthetic signal is set to 30dB. The sampling rate is 1 kHz, and a 4-s data is recorded. The waveform of the synthetic signal is shown in Fig. 2.

$$\boldsymbol{X}=\begin{pmatrix}x_1(t)\\x_2(t)\\x_3(t)\\x_4(t)\end{pmatrix}=\begin{Bmatrix}0.8*s_1(t)+0.9*s_2(t)+1.2*s_3(t)+1.2*s_4(t)\\0.5*s_1(t)+0.6*s_2(t)+0.9*s_3(t)+0.7*s_4(t)\\0.5*s_1(t)+0.6*s_2(t)+0.8*s_3(t)+0.8*s_4(t)\\0.6*s_1(t)+0.5*s_2(t)+0.6*s_3(t)+0.9*s_4(t)\end{Bmatrix} \tag{40}$$

1) *Case 1: Accuracy verification*. Using the proposed MESRT method, the multi-channel global TF matrix of the input signal $\boldsymbol{X}$ in (27) is obtained through (21)-(24). Subsequently, each modal component is reconstructed using (31), and the corresponding oscillation parameters are extracted by the HT method. The TF representation obtained by MESRT is shown in Fig. 3. Fig. 3 demonstrates that the MESRT method significantly improves the accuracy of sub/super-synchronous oscillation parameter identification. By leveraging multi-channel measurement correlations, suppressing noise-induced spurious modes via mean modal energy, and redistributing TF coefficients along instantaneous frequency trajectories using

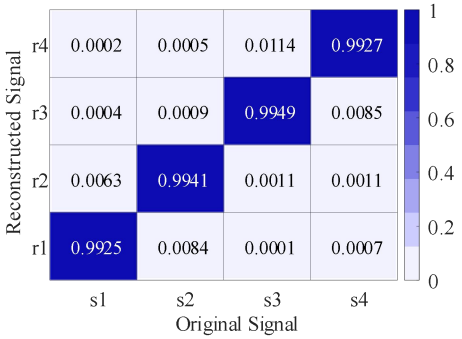

Fig. 5. Correlation between reconstructed and original signals for each mode.

TABLE II
IDENTIFICATION PARAMETERS OF THE SYNTHETIC SIGNAL

Mode	Parameter	Reference value	Identified results	RE/%
1	α	0.3	0.3022	0.7333
	f/Hz	25	24.9922	0.0312
2	α	0.2	0.1991	0.4500
	f/Hz	29	29.0038	0.0131
3	α	0.2	0.2014	0.7000
	f/Hz	71	70.9987	0.0018
4	α	0.3	0.3028	0.9333
	f/Hz	75	75.0092	0.0123

the three-step selection rule, the proposed method concentrates modal energy around the true frequencies (25 Hz, 29 Hz, 50 Hz, 71 Hz, and 75 Hz), thereby mitigating the energy smearing typically observed in existing time-frequency analysis methods.

The time-domain reconstructed signals of the sub/super-synchronous modes are compared with their original counterparts, as shown in Fig. 4. For clarity, only the data from 1s and 1.5s is presented. It is clear that the proposed method accurately decomposes all four modal components, and the reconstructed modes closely match their corresponding original modes. To quantitatively evaluate the reconstruction accuracy, the correlation coefficient is calculated between each reconstructed mode and its original counterpart, as shown in Fig. 5. Fig. 5 shows that all four reconstructed modes exhibit correlation coefficients exceeding 0.99, demonstrating that MESRT provides highly accurate extraction of SSO signals.

For the four extracted sub/super-synchronous oscillation components, the corresponding modal parameters (oscillation frequency f and damping factor α) obtained via the HT method are summarized in Table II. It is clear that, the frequency estimation demonstrates very high accuracy for all four modes, with the maximum relative error of 0.0312% observed in Mode 1. In comparison, the identified damping factors for Modes 1–4 exhibit relative errors of 0.7333%, 0.45%, 0.7%, and 0.9333%, respectively. The slightly larger deviations observed in the damping factor estimation are expected due to its higher sensitivity to noise and signal reconstruction accuracy. Nevertheless, all damping factor errors remain below 1%, indicating excellent agreement with the theoretical values. These results confirm that the proposed MESRT method provides highly accurate and reliable parameter identification of sub/super-synchronous oscillation.

2) *Case 2: Comparison with other methods*. In this case study, the proposed method is compared with STFT-, SET-, FSST- and conventional SRT-based methods in terms of parameter

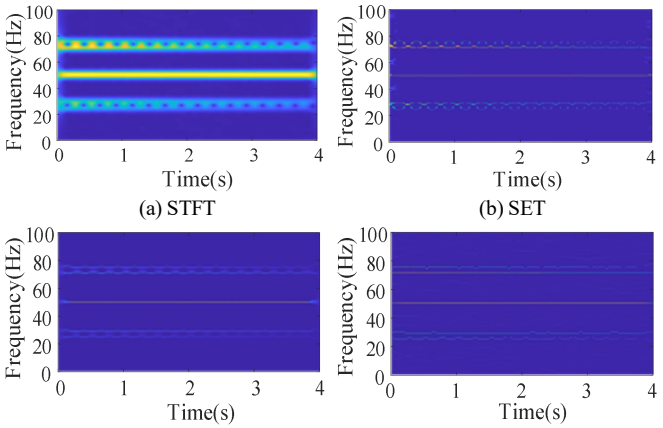

Fig. 6. Comparison of time-frequency analysis results using different methods.

TABLE III

PARAMETER IDENTIFICATION OF THE SYNTHETIC SIGNAL BY DIFFERENT METHODS

Method	α		f	
	Identified value	RE/%	Identified value/Hz	RE/%
Theoretical	0.3	-	25	-
Proposed	0.3022	0.7333	24.9922	0.0312
STFT-HT	0.2911	2.9667	24.9906	0.0376
SET-HT	0.3070	2.3333	24.9912	0.0352
FSST-HT	0.3064	2.1333	24.9918	0.0328
SRT-HT	0.3048	1.6000	24.9920	0.0320
MProny	0.3230	7.6667	24.9901	0.0396

identification accuracy. It should be noted that all four comparative methods are inherently single-channel approaches. Therefore, the best identification results among all measurement channels obtained by each single-channel methods are selected and used for comparison with the proposed method. The time-frequency analysis results for the measured signal in Fig. 2 are shown in Fig. 6. In Fig. 6 (a), STFT exhibits poor time-frequency resolution, resulting in severe energy overlap among oscillation modes. Fig. 6 (b) shows that the SET method mitigates the energy dispersion of STFT through a synchrosqueezing operator; however, noticeable local spreading and significant energy mixing remain. In particular, leakage occurs between the 25 Hz and 29 Hz modes, as well as between the higher-frequency 71Hz and 75 Hz modes, preventing a clean separation of these oscillatory components. Fig. 6(c) shows that FSST effectively concentrates energy around the true modal frequencies by applying a synchrosqueezing operator, but the use of a fixed window leads to unsmooth time-frequency trajectories. Fig. 6(d) reveals that although the traditional SRT enhances smoothness and scale resolution of the TF representation, it does not leverage multi-channel correlations and remains noise sensitive compared with the proposed method in Fig. 3. Consequently, energy diffusion appears in the TFR, hindering the formation of compact and well-defined frequency concentration regions.

Furthermore, the reconstructed time-domain components are analyzed, and oscillation parameters are extracted using the HT method; for brevity, only the best-identified case, namely the 25 Hz mode, is presented. The results are summarized in Table III, together with those obtained from the multi-channel Prony-based approach. Analysis of Table III indicates noticeable differences among the compared methods in both frequency and damping factor estimation. The multi-channel Prony approach exhibits the

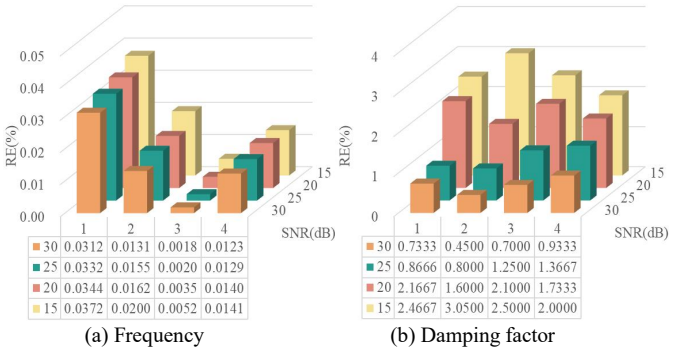

Fig. 7. Frequency and damping factor errors by the proposed method under different SNRs.

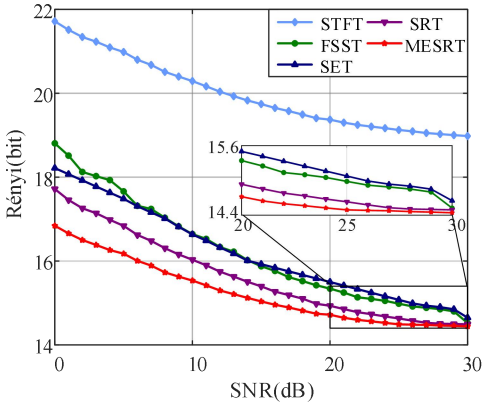

Fig. 8. Rényi entropy of different methods under various noise levels.

largest estimation errors, with damping factor and frequency errors reaching 7.6667% and 0.0396% respectively. This degradation is mainly attributed to its high sensitivity to noise and model mismatch, which may lead to inaccurate modal fitting under noisy conditions. For the time-frequency based approaches, all methods achieve comparable frequency identification, with the maximum error observed in the STFT method being approximately 0.0376%. However, for damping factor identification, the proposed MESRT method yields the smallest relative error. Specifically, the identification errors of damping factors obtained by the proposed MESRT, and by the STFT-, SET-, FSST- and SRT-based methods are 0.7333%, 2.9667%, 2.3333%, 2.1333%, and 1.6000% respectively. The STFT-based method produces the largest damping factor error, indicating its relatively poor time-frequency energy concentration capability. Compared with STFT, the FSST- and SET-based methods reduce the estimation errors due to their enhanced energy concentration mechanisms; however, their performance remains affected by noise contamination. The SRT-based method achieves improved accuracy compared with STFT, SET, and FSST, but its reliance on tracking local maxima makes it susceptible to noise-induced spurious components, which may lead to deviations in modal trajectory extraction. In contrast, the proposed MESRT method achieves the smallest estimation error among all compared approaches. This improvement is mainly attributed to the multi-channel cooperative framework and the modal energy-based threshold strategy, which effectively suppress noise-induced spurious modes and enhance the reliability of oscillation parameter estimation. These results verify that the proposed method provides improved accuracy and enhanced robustness

TABLE IV
MONTE CARLO SIMULATION OF THE SYNTHETIC SIGNAL BY DIFFERENT METHODS

Method	α		f	
	Mean	Variance	Mean/Hz	Variance/Hz^2
Proposed	0.3035	4.41×10^{-4}	24.9982	1.44×10^{-4}
STFT-HT	0.2945	72.25×10^{-4}	25.0064	13.16×10^{-4}
SET-HT	0.3092	38.44×10^{-4}	24.9960	6.25×10^{-4}
FSST-HT	0.3085	30.25×10^{-4}	24.9976	5.76×10^{-4}
SRT-HT	0.3067	8.41×10^{-4}	24.9979	2.56×10^{-4}
MProny	0.3402	121.49×10^{-4}	25.0111	24×10^{-4}

against noise, demonstrating its effectiveness for sub-/super-synchronous oscillation parameter identification.

3) *Case 3: Robustness to noise*. The robustness of the proposed method against noise is evaluated by testing the signal shown in Fig. 2 with the SNR gradually reduced from the initial 30 dB to 25 dB, 20 dB, and 15 dB. The proposed method is then applied to identify the oscillation parameters, and Fig. 7 presents the frequency and damping factor errors for the four sub/super-synchronous oscillation modes. As shown in Fig. 7, both the frequency and damping factor errors increase as the SNR decreases. For frequency estimation, Fig. 7(a) shows that the errors remain extremely small across all noise levels; even under the strongest noise condition (SNR=15 dB), the maximum frequency error remains below 0.0372%. In contrast, the damping factor estimates shown in Fig. 7(b) exhibit higher sensitivity to noise. When the SNR drops to 15 dB, the maximum damping factor error reaches 3.05% for the 29 Hz mode, yet this level of deviation is still acceptable for engineering applications. Such strong noise robustness mainly benefits from the introduction of average modal energy, which effectively suppresses noise-induced spurious modes, and the incorporation of the three-step selection rule, which concentrates the time-frequency energy around the true frequency trajectories, thereby enhancing overall noise resistance.

Furthermore, Gaussian white noise is added to the signal in (40) with an SNR varying from 0 to 30 dB in 2 dB increments. The proposed method is compared with STFT-, SET-, FSST-, and conventional SRT-based methods in terms of oscillation parameter identification performance under varying noise conditions. In addition, the Rényi entropy is employed to quantitatively evaluate the concentration of time-frequency energy in the results. A lower Rényi entropy indicates stronger energy concentration and better accuracy in tracking the true instantaneous frequencies [27]. The Rényi entropy values by the five methods under different SNRs are shown in Fig. 8.

As illustrated in Fig. 8, the Rényi entropy of all methods increases progressively as the noise level increases. Among the compared methods, STFT exhibits the largest Rényi entropy across all SNRs, indicating the poorest energy concentration in its TF representation. The SET estimates instantaneous frequency via a synchroextracting operator, which mitigates mode mixing issue but remains sensitive to noise. FSST enhances localization through synchrosqueezing, thereby improving noise resistance to a certain degree; however, it may still compress noise components erroneously. For the traditional SRT, noise-induced

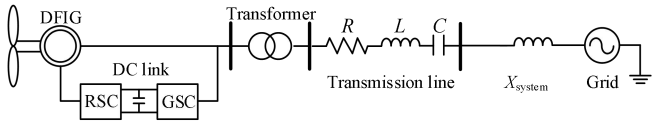

Fig. 9. Equivalent single-machine system diagram.

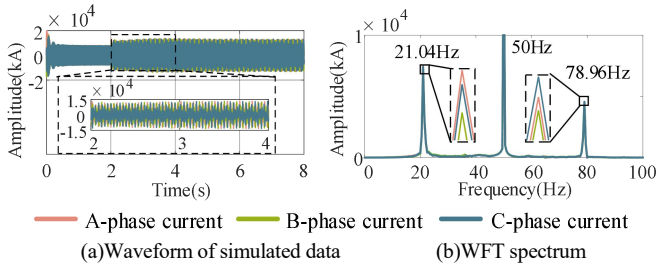

(a)Waveform of simulated data (b)WFT spectrum

Fig. 10. Three-phase current waveforms and their frequency spectra.

TABLE V
IDENTIFICATION RESULTS OF THE SIMULATED SIGNAL USING MESRT

Mode	Parameter	Reference value	Proposed	RE/%
1	α	0.2885	0.2897	0.4159
	f/Hz	21.0357	21.0428	0.0133
2	α	0.2356	0.2372	0.6791
	f/Hz	78.9529	78.9591	0.0079

spurious modes may generate false local extrema, leading to degraded accuracy under low-SNR conditions. In contrast, the proposed method consistently achieves the lowest Rényi entropy across all SNRs, with the improvement becoming more pronounced under high-noise conditions. These results clearly demonstrate the proposed method exhibits superior robustness and accuracy in identifying sub/super-synchronous oscillation parameters even under severe noise conditions.

4) *Case 4: Monte Carlo statistical evaluation*. To further statistically evaluate the identification accuracy and robustness of the proposed method, a Monte Carlo simulation is conducted. In this study, the synthetic signal described in (39) is used as the test signal. Gaussian white noise with an SNR of 30 dB is added to the signal, and independent noise realizations are generated in each trial to emulate measurement uncertainty. A total of 200 independent trials are conducted. In each trial, the oscillation parameters, including the oscillation frequency and damping factor, are estimated using the proposed MESRT method, as well as the STFT-, SET-, FSST-, multi-channel Prony- and conventional SRT-based approaches. The mean and standard deviation of the estimation errors are then calculated to statistically evaluate the identification performance of each method.

Table IV summarizes the Monte Carlo results for the 25 Hz oscillation mode. It can be observed that the proposed MESRT method achieves the smallest mean estimation errors and the lowest standard deviations for both the oscillation frequency and damping factor among the compared methods. These results indicate that the proposed method provides not only higher identification accuracy but also improved statistical stability under noisy measurement conditions.

TABLE VI
RELATIVE ERRORS OF PARAMETER IDENTIFICATION FOR SIMULATED SIGNALS USING VARIOUS METHODS UNDER DIFFERENT NOISE LEVELS

		RE/%											
Noise level/dB		Mode 1						Mode 2					
		Proposed	STFT	SET	FSST	SRT	MProny	Proposed	STFT	SET	FSST	SRT	MProny
30	α	0.6932	2.6690	2.2877	1.9757	1.6984	10.0173	1.5705	3.8200	3.0560	2.1647	1.7403	10.4652
	f	0.0352	0.0894	0.0822	0.0737	0.0551	0.1017	0.0086	0.0331	0.0205	0.0179	0.0095	0.0399
25	α	1.0399	2.8076	2.5997	2.2184	2.0104	13.5529	1.6553	4.2869	3.6927	2.6316	1.8251	14.5586
	f	0.0456	0.0965	0.0898	0.0784	0.0575	0.1117	0.0092	0.0333	0.0247	0.0196	0.0124	0.0454
20	α	1.1438	3.1889	2.9116	2.4957	2.1837	19.4107	1.7827	4.6689	4.0323	3.7351	2.0798	20.5433
	f	0.0461	0.1022	0.0922	0.0822	0.0594	0.1307	0.0096	0.0339	0.0262	0.0214	0.0152	0.0512
15	α	1.3521	3.7088	3.2236	2.9116	2.3917	27.3830	1.9525	5.6027	4.6265	4.3718	3.0136	32.9117
	f	0.0479	0.1112	0.0998	0.0865	0.0656	0.1602	0.0100	0.0353	0.0282	0.0236	0.0199	0.0564

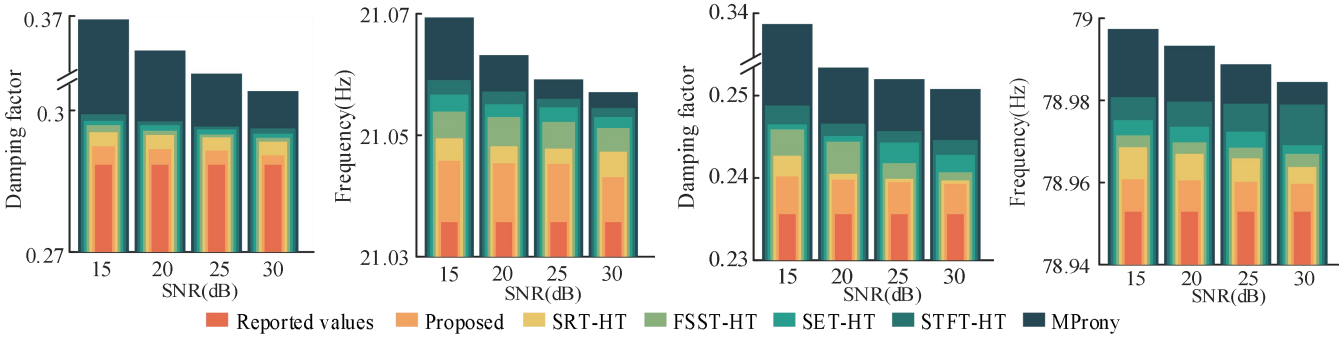

(a)Damping factor of Mode 1 (b)Frequency of Mode 1 (c)Damping factor of Mode 2 (d)Frequency of Mode 2

Fig. 11. Identification results of different methods under different SNRs.

B *Simulated Oscillation Signals*

In this section, the proposed method is validated using simulated SSO data. A grid-connected doubly fed induction generator (DFIG)-based wind farm with a series-compensated transmission line is modeled in MATLAB/Simulink, as shown in Fig. 9. The equivalent wind farm consists of 66 DFIGs, each rated at 1.5 MW. Key parameters are provided in the Appendix, and detailed information of the simulation model can be found in [20]. The initial wind speed is set to 11 m/s, and the series compensation level is 10%.

In the simulation scenario, the system operates under steady-state conditions until a SSO is excited when the series compensation level increases from 10% to 45% at t=2 s. The oscillation is triggered by the electrical resonance between the transmission-line series capacitor and the inductance of the remaining system. The three-phase current waveform at the DFIG terminal are analyzed over a 8-s data window, as shown in Fig. 10 (a). The data between 2 s and 4 s are used for further analysis. The windowed Fourier transform (WFT) with a frequency resolution of 0.5Hz is then applied. The resulting WFT spectrum in Fig. 10 (b) reveals, in addition to the fundamental component, a pair of sub- and super-synchronous oscillation modes at 21.04 Hz and 78.96 Hz respectively.

The proposed MESRT method is applied to the simulated data between 2s and 4 s, to obtain the parameters of each oscillation component. Since the true oscillation parameters in the model-based simulation are unknown, the variational mode decomposition combined with the HT (VMD-HT) method is employed as a benchmark [14]. The identification results of both methods are summarized in Table V. Additionally, the proposed method is compared with STFT-, SET-, FSST-, and traditional SRT-based methods, as well as multi-channel Prony method, under different noise levels. The corresponding results are listed in Table VI and Fig. 11.

As shown in Table V, the proposed method accurately identifies two sub/super-synchronous modes at 21.0428 Hz and 78.9591 Hz from the simulated data, which is consistent with the spectral observations in Fig. 10 (b). The maximum identification errors in oscillation frequency and damping factor are only 0.0133% and 0.6791% respectively, indicating a high level of estimation accuracy. Such high identification accuracy is mainly attributed to the multi-channel cooperative framework and the modal energy-based threshold strategy, which effectively suppress noise-induced spurious modes and improve the reliability of oscillation component extraction. Consequently, the identified results closely align with the benchmark values, further confirming the effectiveness of the proposed method in extracting oscillation parameters.

As summarized in Table VI and Fig. 11, it can be observed that as the SNR decreases from 30 dB to 15 dB, the identification accuracy of all methods deteriorates to different extents for both frequency and damping factor estimation, with damping factor showing higher sensitivity to noise. In particular, at an SNR of 15 dB, the damping factor errors of mode 2 obtained by the proposed method, STFT-, SET-, FSST-, SRT-based and multi-channel Prony methods are 1.9525%, 5.6027%, 4.6265%, 4.3718%, 3.0136% and 32.9117% respectively, indicating that the proposed method maintains the highest accuracy even under strong noise conditions. Among the comparative methods, multi-channel Prony method exhibits the poorest performance, with the error reaching 32.9117% for Mode 2, reflecting its poor noise immunity. For the STFT method, the frequency and damping factor errors are 0.1112% and 3.7088% for mode 1, and 0.0353% and 5.6027% for mode 2, although it performs better than the multi-channel Prony method, noticeable errors still exist. The

improved variants of STFT (SET, FSST, and SRT) show improved accuracy due to enhanced time-frequency energy concentration; however, their estimation errors remain larger than those of the proposed method. Therefore, it can be concluded that the proposed method achieves precise and noise-resilient identification of sub/super-synchronous oscillation parameters.

C Measurement Data from an Actual SSO Event

The proposed method is further validated using measured data recorded during an actual SSO event occurred in the North China power grid [8]. The oscillation was triggered by the interaction between permanent magnet direct-drive wind turbines and a weak grid, with the detailed system topology described in [8]. Fig. 12 (a) shows the measured A-Phase and C-phase current waveforms over a 10-s period following the event, sampled at 1 kHz. The data from 4 to 6 s are selected for analysis, and the corresponding WFT spectrum is presented in Fig. 12 (b). The spectrum clearly reveals a distinct sub-synchronous component around 8.3 Hz in addition to the fundamental component.

The proposed MESRT method is applied to the selected measurement data, and the resulting time-frequency representation is shown in Fig. 13. It can be observed that the proposed method accurately tracks the instantaneous frequencies of the two dominant modes, with strong energy concentrations near 8.3 Hz and 50 Hz. These results are consistent with the WFT spectrum in Fig. 12 (b), confirming the validity the extracted modal parameters.

Subsequently, the time-domain oscillatory components are reconstructed, the oscillation frequency and damping factor of each mode are identified using the HT method. The corresponding identification results are summarized in Table VII and Fig. 14. For comparison, the results obtained using the STFT-HT, SET-HT, FSST-HT, SRT-HT and multi-channel Prony methods are also listed, while the reference values reported in [28] serve as benchmarks. As shown in Table VII and Fig. 14, the dominant oscillation mode associated with the actual SSO event exhibits a frequency of 8.2765 Hz and a damping factor of 0.2287. The results obtained by the proposed method closely match the reported values in [28], with corresponding frequency and damping factor errors of 0.0072% and 0.6559% respectively. In contrast, the five comparative methods yield larger deviations. Among them, the multi-channel Prony method produces the largest identification errors, with the errors of 0.0918% and 16.3096% for frequency and damping factor respectively, followed by the STFT-HT, SET-HT, FSST-HT and SRT-HT methods. These results indicate that the proposed method can accurately identify the SSO signals in an actual power system.

D Comparison of Computational Efficiency

Table VIII summarizes the computation times of different identification methods, including the proposed method, conventional SRT-HT, FSST-HT, SET-HT, STFT-HT, and the multi-channel Prony (MProny) methods. All simulations were conducted in MATLAB® version 2022b on a computing platform equipped with an Intel Core i7-13650HX @ 2.60 GHz processor and 8 GB RAM. As shown in Table VIII, the STFT-

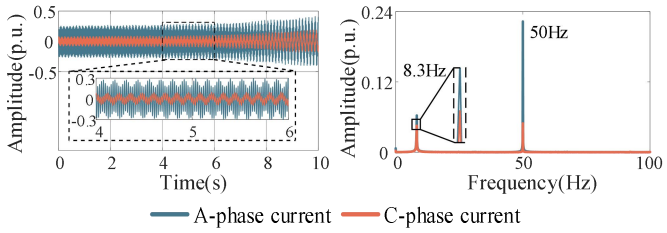

(a) Waveform of simulated data (b) WFT spectrum

Fig. 12. Two-phase current waveforms and their frequency spectra.

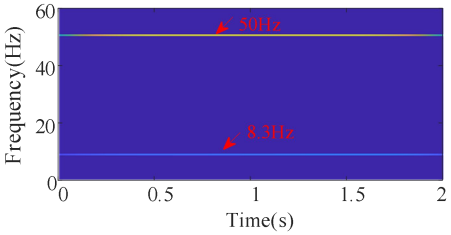

Fig. 13. Time-frequency representation of the measured data using MESRT.

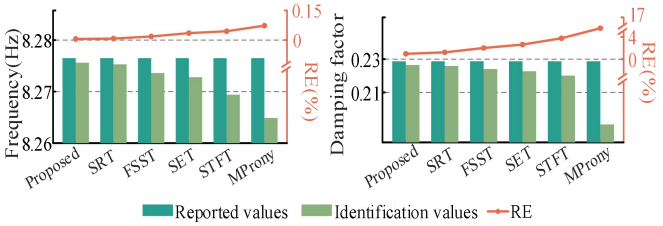

(a) Frequency (b) Damping factor

Fig. 14. Comparison of identification results using different methods.

TABLE VII
PARAMETER IDENTIFICATION RESULTS OF THE MEASURED SIGNAL BY DIFFERENT METHODS

Method	α		f	
	Identified value	RE/%	Identified value/Hz	RE/%
Reported values [28]	0.2287	-	8.2765	-
Proposed	0.2272	0.6559	8.2759	0.0072
STFT-HT	0.2201	3.7604	8.2694	0.0858
SET-HT	0.2227	2.6235	8.2728	0.0447
FSST-HT	0.2241	2.0114	8.2736	0.0350
SRT-HT	0.2259	1.2243	8.2753	0.0145
MProny	0.1914	16.3096	8.2689	0.0918

HT method yields the shortest computation time, with reductions of 70.96%, 66.02% and 69.04% compared with the proposed method for synthetic signals, simulated oscillation signals and actual SSO event respectively; however, its identification accuracy degrades significantly. The improved variants of STFT (e.g., SET, FSST and SRT) exhibit comparable computation times. Due to the introduction of time-frequency energy concentration techniques, their computation times increase noticeably compared with the conventional STFT, with increase of 51.68%, 46.66%, and 48.57% for FSST, 49.31%, 45.47%, and 48.50% for SET, and 46.69%, 40.02%, and 45.86% for SRT, for synthetic signals, simulated oscillation signals, and the actual SSO event, respectively. Nevertheless, these three methods still require less computation time than the proposed method. This is mainly because the proposed method employs a multi-channel cooperative framework and an energy-threshold based strategy to suppress noise-induced spurious modes, thereby significantly improving identification accuracy at the cost of additional computation time. Among all comparative methods, the multi-channel Prony method requires the longest computation time,

TABLE VIII
COMPARISON OF COMPUTATION TIMES FOR DIFFERENT METHODS

Method	Synthetic Signals/s	Simulated Oscillation Signals/s	Actual SSO Event/s
MESRT-HT	1.4374	1.0937	1.2353
SRT-HT	0.7830	0.6195	0.7065
FSST-HT	0.8639	0.6967	0.7438
SET-HT	0.8235	0.6815	0.7427
STFT-HT	0.4174	0.3716	0.3825
MProny	2.3841	1.9496	2.1496

reaching 2.3841 s, 1.9496 s, and 2.1496 s for the three cases respectively, mainly due to the computational burden associated with high-order matrix construction and eigenvalue decomposition inherent in the Prony-based estimation.

CONCLUSION

This paper proposes a multi-channel enhanced synchro-reassignment transform (MESRT) combined with a Hilbert transform-based identification scheme for extracting sub/super-synchronous oscillation parameters from multiple PMU measurements. By extending the conventional single-channel SRT to a multi-channel cooperative framework, MESRT exploits spatial measurement correlations and mean modal energy to suppress noise-induced spurious modes. The three-step selection rule further enhances energy aggregation along instantaneous frequency trajectories, alleviating the scale-blurring issue inherent in conventional time-frequency representations. Case studies using synthetic, simulated and real measured data demonstrate that the proposed method consistently achieves improved parameter identification accuracy and maintains stable performance under low-SNR conditions compared with the STFT-, SET-, FSST- and conventional SRT-based approaches. In addition, relative to conventional multi-channel Prony approach, the proposed method provides more robust and consistent identification results for sub-/super-synchronous oscillations, particularly under noisy measurement conditions.

The proposed framework offers an effective solution for sub-/super-synchronous oscillation monitoring, where noise-contaminated PMU measurements pose significant challenges. By enabling reliable multi-channel parameter extraction with enhanced robustness against measurement noise, this work provides technical support for wide-area oscillation monitoring, early warning, and stability assessment in modern power systems.

APPENDIX A

The parameters of the simulated DFIG-based wind farm system in Section IV.B are adopted from the benchmark model reported in [20]. The detailed values are listed in Tables AI, AII and AIII.

APPENDIX B

This appendix discusses the rationale for selecting the relative modal energy weight threshold μ_0 in this paper, based on three types of data considered in Section IV, including synthetic signals, simulated oscillation signals and actual measurement data. The values of μ_0 are chosen as 0.01, 0.02 and 0.03 for the three respective case studies.

TABLE AI
SYSTEM PARAMETERS

Parameter	Value
System voltage	110 kV
Transformer voltage	110 kV/690 V
Equivalent system reactance, X_{sysem}	19.98 Ω
Transmission line inductance, L	1.32 H
Transmission line resistance, R	5.12Ω
Series capacitance, C	76.55 μF

TABLE AII
GENERATOR PARAMETERS

Parameter	Value	Parameter	Value
Nominal voltage	690 V	DC link nominal voltage	1200V
Stator resistance	0.023 p.u.	Magnetizing reactance	3.1 p.u.
Stator reactance	0.3012 p.u.	Inertia constant	0.685
Rotor resistance	0.016 p.u.	Viscous friction coefficient	0.01
Rotor reactance	0.2058p.u.	Number of pole pairs	3

TABLE AIII
DFIG CONTROLLER PARAMETERS

Parameter	Value
Proportional gain of DC-link voltage controller, $K_{p,dc}$	2.23
Integral gain of DC-link voltage controller, $K_{i,dc}$	280.29
Proportional gain of RSC current controller, $K_{p,RSC}$	0.1
Integral gain of RSC current controller, $K_{i,RSC}$	8.11
Proportional gain of GSC current controller, $K_{p,GSC}$	9.01
Integral gain of GSC current controller, $K_{i,GSC}$	603.36

1. Synthetic Signals

The synthetic signal consists of two pairs of sub- and super-synchronous oscillation modes with frequencies of 25 Hz, 29 Hz, 71 Hz, and 75 Hz, along with the fundamental frequency component. To emulate a relatively severe noise environment, additive Gaussian white noise with an SNR of 15 dB is introduced. Under such conditions, (i) additional noise-induced spurious modes may appear, and (ii) these spurious modes may occupy relatively large modal energy weights. Therefore, the determination of μ_0 is illustrated under the SNR of 15 dB. The synthetic signal is first processed using STFT for each measurement channel, and the resulting time-frequency matrices are combined to form a global multi-channel time-frequency matrix. The relative modal energy weights at each frequency are then calculated, the corresponding results are shown in Fig. B1.

For synthetic signals, it can be clearly observed from Fig. B1 that with a threshold of 0.01, the relative modal energy weights at the inherent sub- and super-synchronous oscillation frequencies exceed threshold μ_0. However, the energy weights corresponding to spurious modes (e.g., spurious mode 2 and spurious mode 4) also exceed threshold μ_0 and are thus incorrectly retained. This is attributed to the relatively small threshold μ_0, which is insufficient to effectively suppress noise-induced

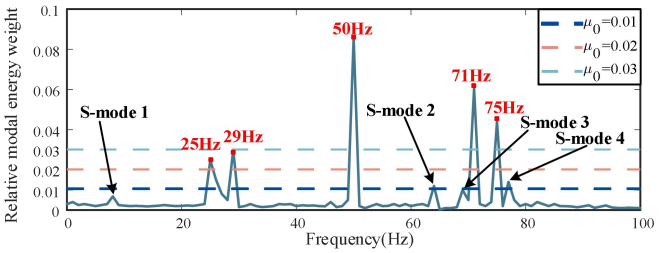

Fig.B1 Relative modal energy weights at each frequency of the synthetic signals.

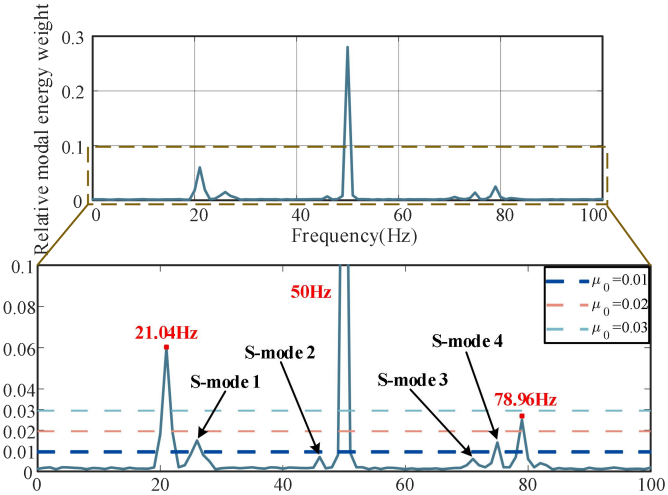

Fig.B2 Relative modal energy weights at each frequency of the simulated signals.

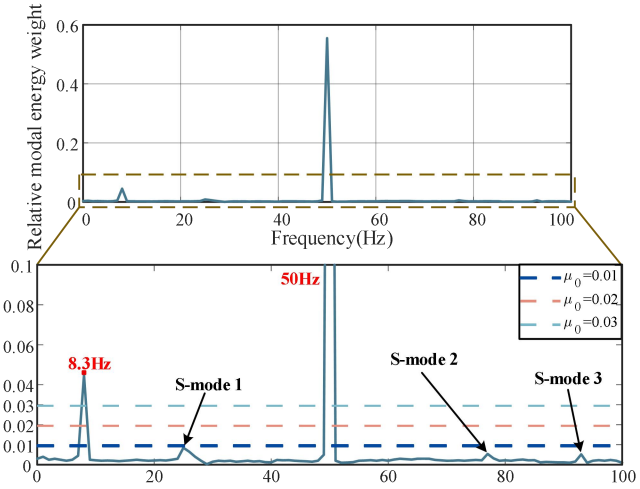

Fig.B3 Relative modal energy weights at each frequency of the actual SSO event.

components. When μ_0 is set to 0.02, only the four true sub- and super-synchronous oscillation modes are preserved, which is consistent with the actual oscillation frequencies of the synthetic signal. When μ_0 is further increased to 0.03, the relative energy weights corresponding to the sub-synchronous oscillation frequencies of 25 Hz and 29 Hz become smaller than μ_0 and are thus incorrectly eliminated, which is caused by an excessively large threshold μ_0.

2. Simulated Oscillation Signals

As described in Section IV.B, the simulated sub-/super-synchronous oscillation signal contains oscillation modes at 21.04 Hz and 78.96 Hz, along with the 50 Hz fundamental component. Additionally, Gaussian white noise with an SNR of 15 dB is added to the oscillation signal. The STFT is applied to the simulated signals, and the multi-channel joint time-frequency matrix is constructed. The relative modal energy weights of each frequency band are then calculated, with the results shown in Fig. B2.

It is clear that, for the simulated signals, when the threshold μ_0 is set to 0.01, the relative mode energy weights of the spurious mode 1 and spurious mode 4 exceed threshold μ_0, preventing its effective removal. This is likely due to the excessively small threshold μ_0, which causes noise-induced spurious modes to be incorrectly retained as real oscillation modes. When μ_0 is set to 0.02, the sub-synchronous mode at 21.04 Hz and the super-synchronous mode at 78.96 Hz are accurately preserved. However, when μ_0 is set to 0.03, the relative mode energy weight of the super-synchronous mode at 78.96 Hz becomes smaller than threshold μ_0, leading to its incorrect removal. This issue is attributed to the relatively large threshold μ_0.

3. Measurement Data from an Actual SSO Event

An actual SSO event with a frequency of 8.3 Hz occurred in the North China power grid. The STFT is applied to the measurement signal of each channel to obtain the corresponding time-frequency coefficient matrices, and a global multi-channel time-frequency matrix is constructed. The relative modal energy weight at each frequency band is then calculated, and the results are shown in Fig. B3. It is evident that, for all threshold values of μ_0 (0.01, 0.02 and 0.03), the sub-synchronous oscillation mode at 8.3 Hz is consistently preserved, without introducing additional noise-induced spurious modes. This result aligns with the actual system behavior.

Based on the results shown in Figs B1-B3, it can be concluded that a relatively small threshold μ_0 may lead to the retention of noise-induced spurious modes from the measurements, whereas an excessively large μ_0 may result in the loss of true sub-/super-synchronous oscillation modes. Therefore, by setting μ_0 to 0.02 across all cases, the proposed method can effectively preserve the dominant sub-/super-synchronous oscillation modes without introducing irrelevant noise-induced spurious components.

REFERENCES

[1] N. Modi, E. M. Farahani, A. Jalali, J. Ramamurthy, C. Chin and B. Soetantijo, "Replication of real-world sub-synchronous oscillations in inverter-based resources dominated grid," *IEEE Trans. Power Del.*, vol. 39, no. 3, pp. 1399–1406, Jun. 2024.

[2] Y. Xu, Y. Cheng, L. Zheng and H. Liu, "A criterion for oscillation source localization with IBRs based on sub-synchronous frequency component of instantaneous power," *IEEE Trans. Power Syst.*, vol. 39, no. 6, pp. 7346–7358, Nov. 2024.

[3] Y. Cao, X. Du, J. Liu, H. -M. Tai, C. Du and X. Zou, "Characterizing sub-synchronous oscillation propagation in MMC-MTDC system based on SSO propagation coefficients," *IEEE Trans. Power Syst.*, vol. 39, no. 6, pp. 7025–7037, Nov. 2024.

[4] J. Adams, C. Carter, and S. H. Huang, "ERCOT experience with sub-synchronous control interaction and proposed remediation," in *Proceedings of PES T&D*, Orlando, USA, May 2012, pp. 1–5.

[5] B. Sun, X. Wu, X. Chen and J Zhou, "An identification scheme for wideband oscillation parameters based on AR-EWT and interpolated DFT," *IEEE Trans. Instrum and Meas.*, vol. 74, pp. 1–12, Feb. 2025.

[6] X. Xie, X. Zhang, H. Liu, H. Liu, Y. Li and C. Zhang, "Characteristic analysis of sub-synchronous resonance in practical wind farms connected to series-compensated transmissions," *IEEE Trans. Energy Convers.*, vol. 32, no. 3, pp. 1117–1126, Sep. 2017.

[7] X. Xie, Y. Zhan, H. Liu, W. Li, and C. Wu, "Wide-area monitoring and early-warning of subsynchronous oscillation in power systems with high-

penetration of renewables," *Int. J. Elect. Power Energy Syst.*, vol. 108, pp. 31–39, 2019.

[8] F. Zhang, J. Li, J. Liu, W. Gao and J. He, "An improved interpolated DFT-based parameter identification for sub-/super-synchronous oscillations with synchrophasors," *IEEE Trans. Power Syst*., vol. 38, no. 2, pp. 1714–1727, Mar. 2023.

[9] B. Sun, X. Wu, X. Chen, Z. Zou, Q. Li and B. Ren, "Parameter estimation of sub-/super-synchronous oscillation based on interpolated all-phase fast Fourier transform with optimized window function," *J. Mod. Power Syst. Clean Energy*, vol. 12, no. 4, pp. 1031–1041, Jul. 2024.

[10] L. Chen, W. Zhao, F. Wang, Q. Wang and S. Huang, "An interharmonic phasor and frequency estimator for subsynchronous oscillation identification and monitoring," *IEEE Trans. Instrum. Meas*., vol. 68, no. 6, pp. 1714–1723, Jun. 2019.

[11] X. Zhang, F. Zhang, J. He and W. Gao, "An enhanced matrix pencil method for parameter identification of sub-/super-synchronous oscillations using synchrophasors," *IEEE Trans. Ind. Informat*., vol. 21, no. 2, pp. 1684–1693, Feb. 2025.

[12] D. Yang, H. Gao, G. Cai, Z. Chen, L. Wang, J. Ma, and D. Li, "Synchronized ambient data based extraction of interarea modes using Hankel block-enhanced DMD," *Int. J. Electr. Power Energy Syst.*, vol. 128, 106687, Jun. 2021.

[13] Rubén. O, D. Guillen, F. Carbajal, L. Castro, "An adaptive scheme to improve Prony's method performance to estimate signal parameters of power system oscillations," *IEEE Trans. Instrum. Meas*., vol. 71, 9005212 Jul. 2022.

[14] L. Wang, G. Cai, D. Yang and Z. Sun, "Extracting modes from electromechanical oscillation signals for power system based on adaptive variational mode decomposition," *Power Syst. Technol.*, vol. 43, no. 4, pp. 1387–1395, Feb. 2019.

[15] L. Wang, B. Wang, H. Gao, D. Yang, S. Xia, and T. Lie, "Synchronized data-based identification of electromechanical oscillation modes using improved FastICA considering measurement noise," *IEEE Trans. Instrum. Meas*., vol. 74, 3003413 Jul. 2025.

[16] Y. Avargel and I. Cohen, "Modeling and identification of nonlinear systems in the short-time Fourier transform domain," *IEEE Trans. Signal Process.*, vol. 58, no. 1, pp. 291–304, Jan. 2010.

[17] T. Jiang, L. Bai, G. Li, H. Jia, Q. Hu and H. Yuan, "Estimating inter-area dominant oscillation mode in bulk power grid using multi-channel continuous wavelet transform," *J. Mod. Power Syst. Clean Energy*, vol. 4, no. 3, pp. 394–405, Jul. 2016.

[18] G. Yu, M. Yu, and C. Xu, "Synchroextracting transform," *IEEE Trans. Ind. Electron*., vol. 64, no. 10, pp. 8042–8054, Oct. 2017.

[19] M. He, S. Nimmagadda, S. Bayne and M. Giesselmann, "Subsynchronous oscillation detection using phasor measurements and synchrosqueezing transform," in *Proc. IEEE Power Energy Soc Gen. Meeting*, 2015, pp. 1–5.

[20] Y. Ma, Q. Huang, Z. Zhang and D. Cai, "Application of multisynchrosqueezing transform for subsynchronous oscillation detection using PMU data," *IEEE Trans. Ind. Appl*., vol. 57, no. 3, pp. 2006–2013, May-June. 2021.

[21] I. Daubechies, J. Lu, and H. T. Wu, "Synchrosqueezed wavelet transforms: An empirical mode decomposition-like tool," *Appl. Comput. Harmon. Anal.*, vol. 30, no. 2, pp. 243–261, Mar. 2011.

[22] C. A. MusluoguM. Li, T. Wang, Y. Kong, and F. Chu, "Synchro-reassigning transform for instantaneous frequency estimation and signal reconstruction," *IEEE Trans. Ind. Electron*., vol. 69, no. 7, pp. 7263–7274, Jul. 2022.

[23] P. G. Estevez, P. Marchi, F. Messina and C. Galarza, "Forced oscillation identification and filtering from multi-channel time-frequency representation," *IEEE Trans. Power Syst*., vol. 38, no. 2, pp. 1257–1269, March. 2023.

[24] R. A. Carmona, W. L. Hwang and B. Torresani, "Multiridge detection and time-frequency reconstruction," *IEEE Trans. Signal Process*., vol. 47, no. 2, pp. 480–492, Feb. 1999.

[25] A. R. Messina and V. Vittal, "Nonlinear, non-stationary analysis of interarea oscillations via Hilbert spectral analysis," *IEEE Trans. Power Syst*., vol. 21, no. 3, pp. 1234–1241, Aug. 2006.

[26] IEEE/IEC International Standard—Measuring Relays and Protection Equipment—Part 118-1: Synchrophasor for Power System — Measurements, IEC/IEEE Standard 60255-118-1:2018, 2018, pp. 1–78.

[27] R. G. Baraniuk, P. Flandrin, A. J. E. M. Janssen and O. J. J. Michel, "Measuring time-frequency information content using the Renyi entropies," *IEEE Trans. Inf. Theory*., vol. 47, no. 4, pp. 1391–1409, May 2001.

[28] J. G. Philip, J. Jung and A. Onen, "Empirical wavelet transform based method for identification and analysis of sub-synchronous oscillation modes using PMU data," *J. Mod. Power Syst. Clean Energy*, vol. 12, no. 1, pp. 34–40, January. 2024.

Lixin Wang received the B.S., M.S. and Ph.D. degrees from Northeast Electric Power University, Jilin, China, in 2014, 2017 and 2021 respectively, then worked as a Postdoctoral Fellow there in 2024 and 2025. She was also a Visiting Scholar at Auckland University of Technology, Auckland, New Zealand, in 2025.

Her research interests include power system stability analysis and control, and data-driven situational awareness for renewable power system.

Tianhong Niu received the B.S. degree in electrical engineering and automation from Changchun Institute of Technology, Changchun, China, in 2024. He is currently working toward the M.S. degree in the School of Electrical Engineering, Northeast Electric Power University, Jilin, China.

His research interests include power system stability analysis and control.

Zhenglong Sun received the B.S., M.S., and Ph.D. degrees in electrical engineering from Northeast Electric Power University, Jilin, China, in 2011, 2014, and 2018, respectively. He is currently a Professor with the School of Electrical Engineering, Northeast Electric Power University, Jilin, China.

His research interests include stability analysis and control of renewable power systems.

Han Gao received the B.S. and Ph.D. degrees from Northeast Electric Power University, Jilin, China, in 2017 and 2023, respectively.

Her research interests include machine learning, and data-driven power system stability analysis and control.

Shouqi Jiang received the B.S. and M.S. degrees in Electrical Engineering from Northeast Electric Power University, Jilin, China, in 2014 and 2017, respectively, and the Ph.D. degree in Electrical En gineering from Northeast Electric Power University, Jilin, China, in 2020.

His research interests include renewable energy integration, MMC-HVDC system and DC grid.

Guowei Cai received the B.S.and M.S.degrees from Northeast Electric Power University, Jilin, China, in 1990 and 1993, respectively, and the Ph.D. degree from the Harbin Institute of Technology, Harbin, China, in 1999. Since 2004, he has been a Professor with the School of Electrical Engineering, Northeast Electric Power University.

His research interests include power system transient stability analysis and smart grid with renewable power generation.

Tek Tjing Lie (Senior Member, IEEE) received the B.S. degree in electrical engineering from Oklahoma State University, Stillwater, OK, USA, in 1986 and the M.S. and Ph.D. degrees in electrical engineering from Michigan State University, East Lansing, MI, USA, in 1988 and 1992 respectively.

He is currently a Full Professor and the Head of the School of Engineering, Computer and Mathematical Sciences at Auckland University of Technology, Auckland, New Zealand. He was the Chair of the IEEE New Zealand North Section from 2020 to 2023 and as Vice-Chair in 2024. His research interests include power system operation and control, deregulated electrical power markets, AI applications to power systems, power electronics, renewable energy, and smart grids.